Inorg. Chem. **2008**, *47*, 1674−1686

Transient Intermediates from Mn(salen) with Sterically Hindered Mesityl Groups: Interconversion between Mn^{IV}-Phenolate and Mn^{III}-Phenoxyl Radicals as an Origin for Unique Reactivity

Takuya Kurahashi,[†] Akihiro Kikuchi,[‡] Takehiko Tosha,[†] Yoshitsugu Shiro,[‡] Teizo Kitagawa,[†] and Hiroshi Fujii*[,†]

Institute for Molecular Science & Okazaki Institute for Integrative Bioscience, National Institutes of Natural Sciences, Myodaiji, Okazaki, Aichi 444-8787, Japan, and RIKEN SPring-8 Center, Harima Institute, 1-1-1, Kouto, Sayo, Hyogo 679-5148, Japan

Received October 18, 2007

In order to reveal structure–reactivity relationships for the high catalytic activity of the epoxidation catalyst Mn(salen), transient intermediates are investigated. Steric hindrance incorporated to the salen ligand enables highly selective generation of three related intermediates, O═Mn^{IV}(salen), HO−Mn^{IV}(salen), and H_2O−Mn^{III}(salen$^{+\bullet}$), each of which is thoroughly characterized using various spectroscopic techniques including UV–vis, electron paramagnetic resonance, resonance Raman, electrospray ionization mass spectrometry, ^2H NMR, and X-ray absorption spectroscopy. These intermediates are all one-electron oxidized from the starting Mn^{III}(salen) precursor but differ only in the degree of protonation. However, structural and electronic features are strikingly different: The Mn−O bond length of HO−Mn^{IV}(salen) (1.83 Å) is considerably longer than that of O═Mn^{IV}(salen) (1.58 Å); the electronic configuration of H_2O−Mn^{III}(salen$^{+\bullet}$) is Mn^{III}-phenoxyl radical, while those of O═Mn^{IV}(salen) and HO−Mn^{IV}(salen) are Mn^{IV}-phenolate. Among O═Mn^{IV}(salen), HO−Mn^{IV}(salen), and H_2O−Mn^{III}(salen$^{+\bullet}$), only the O═Mn^{IV}(salen) can transfer oxygen to phosphine and sulfide substrates, as well as abstract hydrogen from weak C−H bonds, although the oxidizing power is not enough to epoxidize olefins. The high activity of Mn(salen) is a direct consequence of the favored formation of the reactive O═Mn^{IV}(salen) state.

Introduction

The reactivity of transition metal ions is considerably dependent on the coordination environment, and thus the design of a ligand system is critically important to achieve desirable reactivity, even by use of the same active metal ion. The most remarkable examples are catalytic oxygenation reactions by porphyrin and salen complexes. In the case of porphyrins, both Mn(porphyrin) and Fe(porphyrin) complexes show high catalytic activity.[1] In contrast, in the case of salens, Mn(salen) complexes are widely utilized as highly reactive epoxidation catalysts,[2,3] while Fe(salen) complexes are known to be poor catalysts. The striking difference between these popular ligands is worth investigating in detail to establish structure–reactivity relationships.

In order to consider what gives rise to the reactivity difference, electronic structures of transient intermediates are of prime importance. It has been well established that, upon reaction with oxidants at low temperature, Fe(porphyrin) complexes generate O═Fe^{IV}(porphyrin) and O═Fe^{IV}(porphyrin$^{+\bullet}$), which are capable of oxidizing organic substrates.[4,5] Mn(porphyrin) complexes also generate

* To whom correspondence should be addressed. E-mail: hiro@ims.ac.jp.
† National Institutes of Natural Sciences.
‡ Harima Institute.

(1) Meunier, B. *Chem. Rev.* **1992**, *92*, 1411–1456.
(2) Srinivasan, K.; Michaud, P.; Kochi, J. K. *J. Am. Chem. Soc.* **1986**, *108*, 2309–2320.
(3) (a) Zhang, W.; Loebach, J. L.; Wilson, S. R.; Jacobsen, E. N. *J. Am. Chem. Soc.* **1990**, *112*, 2801–2803. (b) Irie, R.; Noda, K.; Ito, Y.; Katsuki, T. *Tetrahedron Lett.* **1991**, *32*, 1055–1058. (c) McGarrigle, E. M.; Gilheany, D. G. *Chem. Rev.* **2005**, *105*, 1563–1602.
(4) (a) Groves, J. T.; Haushalter, R. C.; Nakamura, M.; Nemo, T. E.; Evans, B. J. *J. Am. Chem. Soc.* **1981**, *103*, 2884–2886. (b) Balch, A. L.; Latos-Grazynski, L.; Renner, M. W. *J. Am. Chem. Soc.* **1985**, *107*, 2983–2985. (c) Sugimoto, H.; Tung, H.-C.; Sawyer, D. T. *J. Am. Chem. Soc.* **1988**, *110*, 2465–2470. (d) Fujii, H. *J. Am. Chem. Soc.* **1993**, *115*, 4641–4648.
(5) (a) Chin, D.-H.; Balch, A. L.; La Mar, G. N. *J. Am. Chem. Soc.* **1980**, *102*, 1446–1448. (b) Lee, W. A.; Calderwood, T. S.; Bruice, T. C. *Proc. Natl. Acad. Sci. U.S.A.* **1985**, *82*, 4301–4305. (c) Swistak, C.; Mu, X. H.; Kadish, K. M. *Inorg. Chem.* **1987**, *26*, 4360–4366. (d) Groves, J. T.; Gross, Z.; Stern, M. K. *Inorg. Chem.* **1994**, *33*, 5065–5072.

10.1021/ic702061y CCC: $40.75

Published on Web 02/01/2008

O=Mn^{IV}(porphyrin) and O≡Mn^{V}(porphyrin), which show oxidation activity.[6] On the other hand, we recently reported that an Fe(salen) complex does not generate high-valent Fe−oxo species but gives salen phenoxyl radical species, which show no monooxygenation activity.[7]

Transient intermediates from Mn(salen) have also been actively investigated,[8] especially in the context of reactive intermediates for Jacobsen−Katsuki enantioselective epoxidation.[3] By analogy to well-established nonheme high-valent Mn−oxo complexes,[9] O=Mn^{IV}(salen) and O≡Mn^{V}(salen) have been frequently proposed, but the exact identities of transient intermediates still remain elusive. In previous studies, reactions of Mn(salen) with NaOCl, PhIO, or *m*-CPBA (*m*-chloroperbenzoic acid) at low temperatures typically produced mixtures of transient intermediates, which were tentatively assigned as O≡Mn^{V}(salen), Mn^{IV}−O−Mn^{IV} salen dimer, and Mn^{IV}(salen) with O=, HO−, Cl−, *m*-CB−(*m*-chlorobenzoate), and ClO− ligands mainly on the basis of electrospray ionization mass spectrometry (ESI-MS) and electron paramagnetic resonance (EPR) studies. Because more than two species were present in the solution, these assignments were not necessarily reliable, and thus structure–reactivity relationships could not be established. More importantly, our previous study on Fe(salen)[7] suggests that reactions of Mn(salen) with oxidants might also generate salen phenoxyl radical species, as well as high-valent Mn^{V}(salen) or Mn^{IV}(salen), due to comparable oxidation potentials of the central Mn versus the salen ligand. Indeed, many examples have been reported for metal−phenoxyl radical complexes,[10] including Mn−phenoxyl radical complexes.[11]

Transient intermediates from Mn(salen) are also quite interesting as a model for the oxygen-evolving center (OEC) in photosystem II. According to the most recent X-ray crystal structure,[12] photosynthetic oxidation of water to oxygen proceeds at the mononuclear Mn center in the OEC. Highly effective water oxidation is believed to come from the efficient electron transfer from the OEC to the light-induced P_{680}^{+}, which is mediated by a redox-active tyrosyl radical ($Tyr_Z^{\bullet}$).[13] Mn(salen) has a monomeric Mn center with a vacant coordination site for the H_2O binding, and a coordinated phenolate as a tyrosine model. Thus, one-electron oxidation of Mn(salen) provides an opportunity to examine the role of electron transfer in the water oxidation in the OEC.

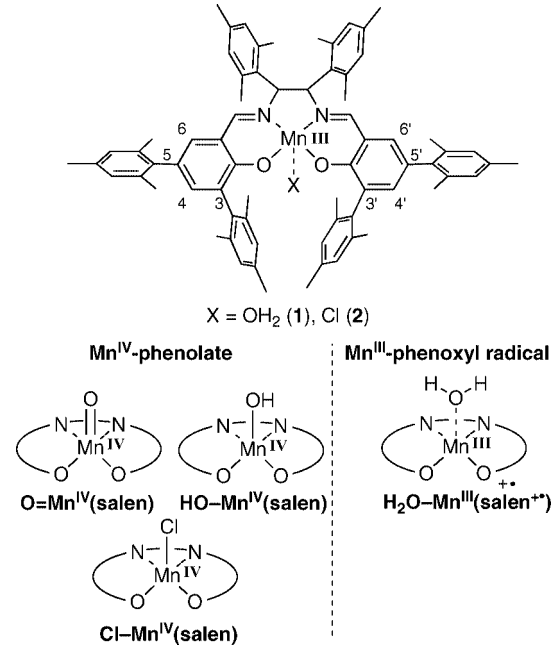

Figure 1. Sterically hindered Mn(salen) **1** and **2**. **1** has ClO_4^- as a counteranion. High-valent Mn^{IV}-phenolate intermediates O=Mn^{IV}(salen), HO−Mn^{IV}(salen), Cl−Mn^{IV}(salen), and Mn^{III}-phenoxyl radical intermediate H_2O−Mn^{III}(salen$^{+\bullet}$) were generated from **1** and/or **2**.

Herein, we prepared sterically hindered Mn(salen) **1** and **2** bearing a protected Mn center (Figure 1), in order to prevent the formation of dimeric species. One-electron oxidation of **1** and **2** generates a Mn^{III}-phenoxyl radical, H_2O−Mn^{III}(salen$^{+\bullet}$), and Mn^{IV}-phenolate, Cl−Mn^{IV}(salen), respectively, which provide a solid spectroscopic basis to distinguish these two electronic configurations. Low-temperature oxidation of sterically hindered **1** enables highly selective generation of possible reactive intermediates, O=Mn^{IV}(salen) and HO−Mn^{IV}(salen), each of which was characterized unambiguously with various spectroscopic methods, including UV–vis, EPR, resonance Raman, ESI-MS, ^{2}H NMR, and X-ray absorption spectroscopy (XAS). Interconversion and energetics among O=Mn^{IV}(salen), HO−Mn^{IV}(salen), and H_2O−Mn^{III}(salen$^{+\bullet}$) explain why Mn(salen) is a far better catalyst than Fe(salen).

(6) (a) Czernuszewicz, R. S.; Su, Y. O.; Stern, M. K.; Macor, K. A.; Kim, D.; Groves, J. T.; Spiro, T. G. *J. Am. Chem. Soc.* **1988**, *110*, 4158–4165. (b) Groves, J. T.; Stern, M. K. *J. Am. Chem. Soc.* **1988**, *110*, 8628–8638. (c) Ayougou, K.; Bill, E.; Charnock, J. M.; Garner, C. D.; Mandon, D.; Trautwein, A. X.; Weiss, R.; Winkler, H. *Angew. Chem., Int. Ed. Engl.* **1995**, *34*, 343–346. (d) Groves, J. T.; Lee, J.; Marla, S. S. *J. Am. Chem. Soc.* **1997**, *119*, 6269–6273. (e) Song, W. J.; Seo, M. S.; George, S. D.; Ohta, T.; Song, R.; Kang, M.-J.; Tosha, T.; Kitagawa, T.; Solomon, E. I.; Nam, W. *J. Am. Chem. Soc.* **2007**, *129*, 1268–1277. (f) Jin, N.; Ibrahim, M.; Spiro, T. G.; Groves, J. T. *J. Am. Chem. Soc.* **2007**, *129*, 12416–12417.

(7) Kurahashi, T.; Kobayashi, Y.; Nagatomo, S.; Tosha, T.; Kitagawa, T.; Fujii, H. *Inorg. Chem.* **2005**, *44*, 8156–8166.

(8) (a) Bryliakov, K. P.; Babushkin, D. E.; Talsi, E. P. *J. Mol. Catal. A: Chem.* **2000**, *158*, 19–35. (b) Feichtinger, D.; Plattner, D. A. *Chem.—Eur. J.* **2001**, *7*, 591–599. (c) Adam, W.; Mock-Knoblauch, C.; Saha-Möller, C. R.; Herderich, M. *J. Am. Chem. Soc.* **2000**, *122*, 9685–9691. (d) Campbell, K. A.; Lashley, M. R.; Wyatt, J. K.; Nantz, M. H.; Britt, R. D. *J. Am. Chem. Soc.* **2001**, *123*, 5710–5719. (e) Feth, M. P.; Bolm, C.; Hildebrand, J. P.; Köhler, M.; Beckmann, O.; Bauer, M.; Ramamonjisoa, R.; Bertagnolli, H. *Chem.—Eur. J.* **2003**, *9*, 1348–1359.

(9) (a) Collins, T. J.; Gordon-Wylie, S. W. *J. Am. Chem. Soc.* **1989**, *111*, 4511–4513. (b) Collins, T. J.; Powell, R. D.; Slebodnick, C.; Uffelman, E. S. *J. Am. Chem. Soc.* **1990**, *112*, 899–901. (c) MacDonnel, F. M.; Fackler, N. L. P.; Stern, C.; O'Halloran, T. V. *J. Am. Chem. Soc.* **1994**, *116*, 7431–7432. (d) Miller, C. G.; Gordon-Wylie, S. W.; Horwitz, C. P.; Strazisar, S. A.; Peraino, D. K.; Clark, G. R.; Weintraub, S. T.; Collins, T. J. *J. Am. Chem. Soc.* **1998**, *120*, 11540–11541. (e) Mandimutsira, B. S.; Ramdhanie, B.; Todd, R. C.; Wang, H.; Zareba, A. A.; Czernuszewicz, R. S.; Goldberg, D. P. *J. Am. Chem. Soc.* **2002**, *124*, 15170–15171. (f) Parsell, T. H.; Behan, R. K.; Green, M. T.; Hendrich, M. P.; Borovik, A. S. *J. Am. Chem. Soc.* **2006**, *128*, 8728–8729.

(10) Chaudhuri, P.; Wieghardt, K. *Prog. Inorg. Chem.* **2001**, *50*, 151–216.

(11) (a) Müller, J.; Kikuchi, A.; Bill, E.; Weyhermüller, T.; Hildebrandt, P.; Ould-Moussa, L.; Wieghardt, K. *Inorg. Chim. Acta* **2000**, *297*, 265–277. (b) Mukherjee, S.; Weyhermüller, T.; Bothe, E.; Wieghardt, K.; Chaudhuri, P. *Dalton Trans.* **2004**, 3842–3853.

(12) Loll, B.; Kern, J.; Saenger, W.; Zouni, A.; Biesiadka, J. *Nature (London)* **2005**, *438*, 1040–1044.

(13) McEvoy, J. P.; Brudvig, G. W. *Chem. Rev.* **2006**, *106*, 4455–4483.

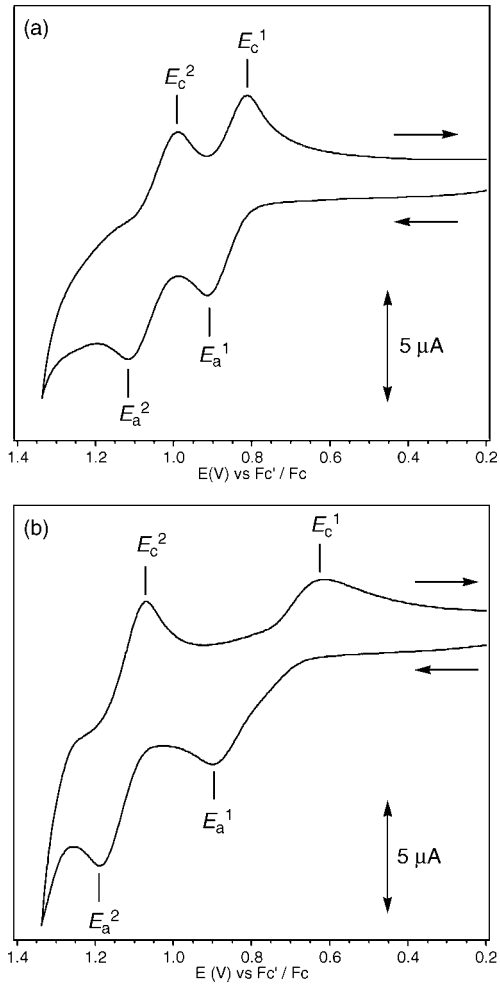

Figure 2. Cyclic voltammograms of (a) **1** and (b) **2** in CH_2Cl_2 at 193 K. Conditions: 1×10^{-3} M **1** or **2**, 0.10 M Bu_4NClO_4 supporting electrolyte, a saturated calomel electrode as a reference electrode, a glassy carbon working electrode, a platinum-wire counter electrode, a scan rate of 50 mV s^{-1}. The potentials are referenced versus the ferrocenium/ferrocene (Fc′/Fc) couple.

Results

Mn^{III}-Phenoxyl Radical from 1. An X-ray crystallographic analysis shows that **1** is a five-coordinate monomeric Mn^{III} complex bearing H_2O as an external ligand and ClO_4^- as a counteranion (Figure S1, Supporting Information). The coordination geometry of **1**, which is close to square-pyramidal, is similar to that of other Mn(salen) complexes.[14,15] Cyclic voltammetry of **1** does not give any clear redox wave at room temperature. But, as shown in Figure 2a, a cyclic voltammogram of **1** at 193 K exhibits two quasi-reversible redox waves, indicating that oxidized derivatives of **1** are stable only at low temperatures. The redox potentials $E_{1/2}^1$ and $E_{1/2}^2$ are 0.86 and 1.06 V versus the ferrocenium/ferrocene couple (Fc′/Fc), respectively. The other parameters are summarized in Table 1. A controlled-potential oxidation of **1** at a voltage (1.0 V) higher than E_a^1 but lower than E_a^2 at 203 K generates an intermediate $[\mathbf{1}]^+$, after

Table 1. Electrochemical Parameters (V) of **1** and **2**[a]

compd	E_a^1	E_a^2	E_c^1	E_c^2	$E_{1/2}^1$	$E_{1/2}^2$
1	0.91	1.12	0.81	0.99	0.86	1.06
2	0.90	1.19	0.62	1.07	0.76	1.13

[a] See the caption in Figure 2 for the measurement conditions.

UV–vis spectral changes with clear isosbestic points, as shown in Figure 3a. The UV–vis spectrum of $[\mathbf{1}]^+$ features a broad absorption centered at 905 nm, along with other absorption maxima at 338, 420, and 550 nm. Electrochemical reduction of $[\mathbf{1}]^+$ at −0.40 V at 203 K regenerates the starting Mn^{III} complex **1**. $[\mathbf{1}]^+$ is also generated by chemical oxidation of **1** using 1.0 equiv of a one-electron chemical oxidant, tris(2,4-dibromophenyl)aminium hexachloroantimonate (**3**). The broad absorption around 905 nm in $[\mathbf{1}]^+$ is closely similar to that for the phenoxyl radicals from Fe(salen),[7] and absorptions at 338 and 420 could be assigned as $\pi-\pi^*$ transitions of the coordinated phenoxyl radical,[10] suggesting that $[\mathbf{1}]^+$ is also a phenoxyl radical intermediate. Further controlled-potential oxidation of $[\mathbf{1}]^+$ at a voltage (1.3 V) higher than E_a^2 at 203 K generates another intermediate, which shows a characteristic absorption of doubled intensity at the wavelength shifted to a lower energy (980 nm) compared with that of $[\mathbf{1}]^+$. This intermediate may correspond to $[\mathbf{1}]^{2+}$, but due to a high oxidation potential, $[\mathbf{1}]^{2+}$ is too unstable to be investigated by other spectroscopic methods.

Resonance Raman spectra of **1** and $[\mathbf{1}]^+$ were measured at the excitation wavelength of 351.4 nm, which may come from the $\pi-\pi^*$ transition of the phenoxyl radical. Consistently, new resonance Raman bands appear at 1485 and 1604 cm^{-1} for $[\mathbf{1}]^+$, while one of two C−O stretching bands at 1273 or 1299 cm^{-1} in **1** disappears and the other shifts to 1283 cm^{-1} (Figure 4). The bands at 1485 and 1604 cm^{-1} for $[\mathbf{1}]^+$ are assigned as Y7a′ and Y8a′ modes, which consist predominantly of C−O stretching and $C_{ortho}-C_{meta}$ stretching, respectively.[10,16] The greater intensity of Y8a′ compared to Y7a′ is consistent with formation of the coordinated phenoxyl radical.[10] **1**-d_4, which is deuterated at positions 4, 6, 4′, and 6′ of the phenolate rings (for numbering, see Figure 1), shows ^2H NMR signals at −1.4 and −58.1 ppm for 6/6′D and 4/4′D of the phenolate moieties, respectively (Figure S2, Supporting Information).[8a,17] In spite of distortion from square-pyramidal, the 6D and 6′D signals as well as the 4D and 4′D signals in **1** show a single ^2H NMR signal due to fast pseudorotation of the salen ligand, which is in contrast to **2**, giving separate signals for both 6/6′D and 4/4′D (*vide infra*). Upon addition of 0.5 and 1.1 equiv of **3** to **1**, these signals gradually disappear, but no apparent signal appears for $[\mathbf{1}]^+$. This is probably because an exchange between phenolate and the phenoxyl radical in $[\mathbf{1}]^+$ via pseudorotation of the salen ligand is comparable to the NMR timescale (∼millisecond), resulting in an extreme line broadening. An ESI-MS spectrum of $[\mathbf{1}]^+$ gives a singly charged signal at *m*/*z* 1128.39, which corresponds to $[Mn(salen)ClO_4]^+$. The ion

(14) Pospisil, P. J.; Carsten, D. H.; Jacobsen, E. N. *Chem.—Eur. J.* **1996**, *2*, 974–980.
(15) Kurahashi, T.; Oda, K.; Sugimoto, M.; Ogura, T.; Fujii, H. *Inorg. Chem.* **2006**, *45*, 7709–7721.
(16) Schnepf, R.; Sokolowski, A.; Müller, J.; Bachler, V.; Wieghardt, K.; Hildebrandt, P. *J. Am. Chem. Soc.* **1998**, *120*, 2352–2364.
(17) Bonadies, J. A.; Maroney, M. J.; Pecoraro, V. L. *Inorg. Chem.* **1989**, *28*, 2044–2051.

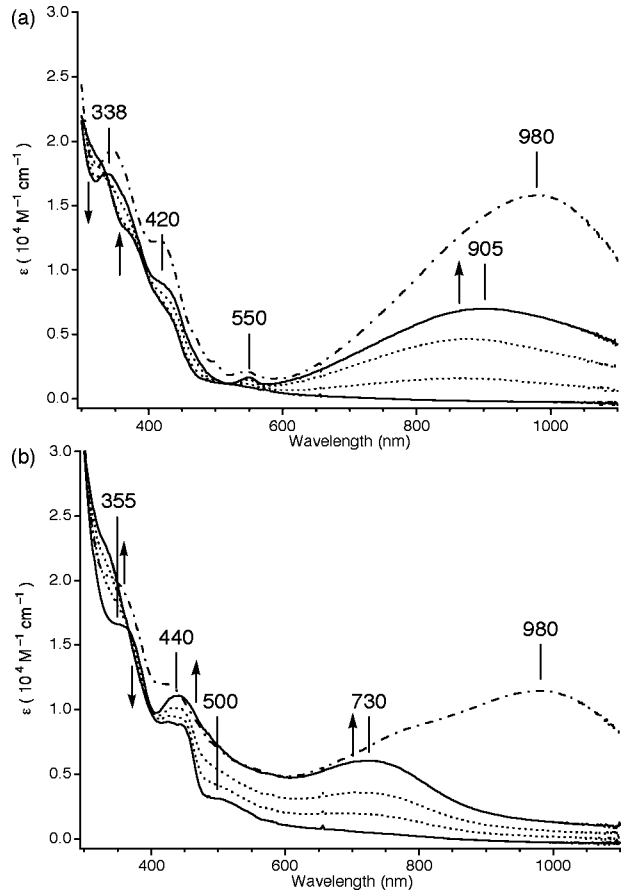

Figure 3. UV–vis spectral changes upon electrochemical oxidation of (a) **1** to $H_2O-Mn^{III}(salen^{+\bullet})$ and (b) **2** to $Cl-Mn^{IV}(salen)$ in CH_2Cl_2 at 203 K. Conditions: 0.5×10^{-3} M **1** or **2**; 0.10 M Bu_4NClO_4 supporting electrolyte; controlled-potential oxidation at 1.00 V vs Fc′/Fc. **1**, $H_2O-Mn^{III}(salen^{+\bullet})$, **2**, and $Cl-Mn^{IV}(salen)$ are depicted as a solid line. UV–vis spectra depicted as a dashed-dotted line are obtained after controlled-potential oxidation at 1.30 V vs Fc′/Fc.

peak corresponding to $[Mn(salen)(H_2O)ClO_4]^+$ is not observed, because the H_2O ligand is easily lost upon ionization.

Figure 5 shows EPR spectra of $[\mathbf{1}]^+$ measured at various temperatures, which clearly shows two sets of signals at $g = 4.70$, 3.00, and 1.85 and $g = 5.82$, 1.23, and 1.16.[18] Their temperature dependence indicates that the signals at $g = 5.82$, 1.23, and 1.16 arise from the ground Kramers doublet, while the signals at $g = 4.70$, 3.00, and 1.85 originate from the excited-state doublet. Linear least-squares fits for signal intensities versus temperature show a negative zero-field splitting value $D = -3$ cm^{-1} (Figure S3, Supporting Information). These signals are derived from an $S_t = {}^3/_2$ spin system ($E/D \approx 0.18$). The $S_t = {}^3/_2$ spin system observed for the Mn^{III}-phenoxyl radical complex could be explained by an antiferromagnetic coupling between the Mn^{III} center ($S = {}^4/_2$) and the phenoxyl radical ($S = {}^1/_2$) on the salen ligand.[11a] Signals at $g = 4.70$ and 5.82 exhibit a six-line hyperfine splitting with $A = 82.1$ and 54.8 G, respectively, as expected for the $I = {}^5/_2$ ^{55}Mn nucleus. The starting complex **1**, which is a d^4 Mn^{III} system, shows a weak, but well-detectable, signal at $g = 7.2$ (Figure S4, Supporting Information). According to the previous perpendicular- and parallel-mode EPR study of Jacobsen's Mn(salen),[8d] this signal was assigned as the transition between the $M_s = \pm 2$ level of an $S = 2$ electron spin system, and the simulation and temperature dependence of the signals indicated $D = -2.5$ cm^{-1} for Jacobsen's Mn^{III}(salen). Variable-temperature EPR in the range of 2.3–50 K shows that the signal at $g = 7.2$ for **1** obeys the Curie law just as in the case of Jacobsen's Mn^{III}(salen), indicative of a negative D value also for **1**. Then, the sign of the zero-field splitting value D remains negative before and after one-electron oxidation of **1**. The accumulated spectroscopic evidence clearly shows that $[\mathbf{1}]^+$ is a Mn^{III}-phenoxyl radical, $H_2O-Mn^{III}(salen^{+\bullet})$.

(18) Two additional signals, which were observed at a higher magnetic field ($g = 0.84$ and 0.56), could not be assigned.

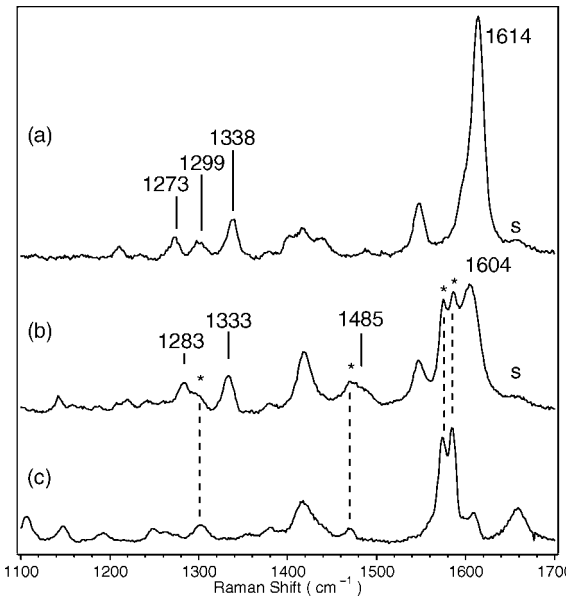

Figure 4. Resonance Raman spectra of a 2 mM solution of (a) **1**, (b) $H_2O-Mn^{III}(salen^{+\bullet})$ generated from **1** + 1.0 equiv of **3**, and (c) reduced **3** generated from **3** + 1.0 equiv of ferrocene in CD_2Cl_2 at 193 K. The excitation wavelength is 351.4 nm. The band from CD_2Cl_2 is denoted with "s". The band designated with an asterisk comes from a reduced **3**.

Mn^{IV}-Phenolate from 2. Cyclic voltammetry of **2** does not give any clear redox wave at room temperature but gives two quasi-reversible redox waves at 193 K (Figure 2b), indicating that oxidized derivatives of **2** are also stable at low temperatures. The first redox potential ($E_{1/2}{}^1$) is 0.76 V versus Fc′/Fc, while the second redox potential ($E_{1/2}{}^2$) is 1.13 V versus Fc′/Fc. As shown in Table 1, the ΔE value for the first redox cycle of **2** is 0.28 V, which is much larger than the value of 0.10 V for the phenolate−phenoxyl radical redox couple in **1**. A controlled-potential oxidation of **2** at 1.0 V leads to UV–vis spectral changes with two isosbestic points, as shown in Figure 3b. The UV–vis spectrum of the transient intermediate $[\mathbf{2}]^+$ shows characteristic absorption maxima at 440 and 730 nm. These spectral changes are completely reversible, and the starting spectrum of **2** is regenerated, when a potential of −0.30 V is applied at 203 K. The addition of 1.0 equiv of **3** to the CH_2Cl_2 solution of **2** also generates exactly the same species. The UV–vis spectrum of $[\mathbf{2}]^+$ is considerably different from that of $H_2O-Mn^{III}(salen^{+\bullet})$, suggesting that $[\mathbf{2}]^+$ is a Mn^{IV} species. Further controlled-potential oxidation of $[\mathbf{2}]^+$ at a voltage (1.3 V) higher than

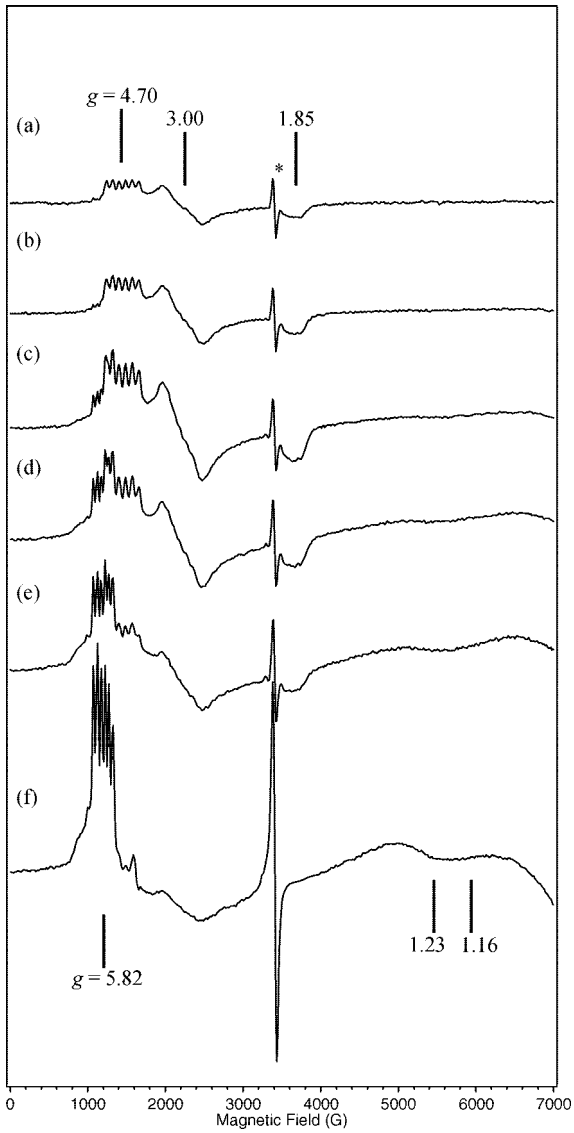

Figure 5. X-band EPR spectra of $H_2O-Mn^{III}(salen^{+\bullet})$ generated from **1** + 1.0 equiv of **3** in frozen CH_2Cl_2-toluene (7:3). Conditions: temperature, (a) 50 K, (b) 30 K, (c) 10 K, (d) 6 K, (e) 4 K, and (f) 2.3 K; microwave frequency, 9.56 GHz; microwave power, 2.012 mW; modulation amplitude, 7 G; time constant, 163.84 ms; conversion time, 163.84 ms. The sharp signal designated with an asterisk comes from remaining **3**.

E_a[2] at 203 K shows UV–vis spectral changes without clear isosbestic points, suggesting that some reactions other than one-electron oxidation occur in this process. The resulting intermediate, which shows a broad absorption at 980 nm similar to $[\mathbf{1}]^{2+}$, is also too unstable to be investigated by other spectroscopic methods.

A resonance Raman spectrum of $[\mathbf{2}]^+$ does not show the band near 1485 cm^{-1}, which is assigned to Y7a′ of the phenoxyl radical in $H_2O-Mn^{III}(salen^{+\bullet})$ (Figure S5, Supporting Information). **2-***d*$_4$ shows separate signals for 4/4′D and 6/6′D at −42.0/−47.9 and 11.5/4.5 ppm, respectively (Figure 6).[8a,17] Because of distortion from square-pyramidal and slow pseudorotation of a salen ligand of **2**, ^{2}H NMR signals for two phenolate rings in **2** are observed at different positions. While ^{2}H NMR signals for $H_2O-Mn^{III}(salen^{+\bullet})$ are not detected, $[\mathbf{2}\text{-}d_4]^+$ shows well-resolved signals at −32.5/−60.3 ppm for 4/4′D and 25.2/−3.8 ppm for 6/6′D.

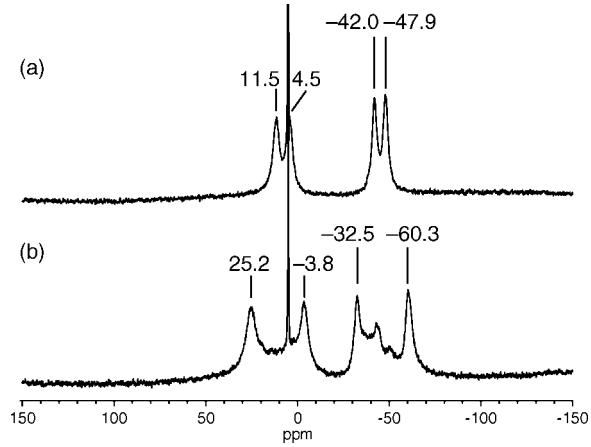

Figure 6. ^{2}H NMR spectra of a 10 mM solution of (a) **2-***d*$_4$ and (b) $Cl-Mn^{IV}(salen)$-*d*$_4$ generated from **2-***d*$_4$ + 1.1 equiv of **3** in CH_2Cl_2 at 203 K. ^{2}H NMR shifts are referenced to CD_2Cl_2 (5.32 ppm).

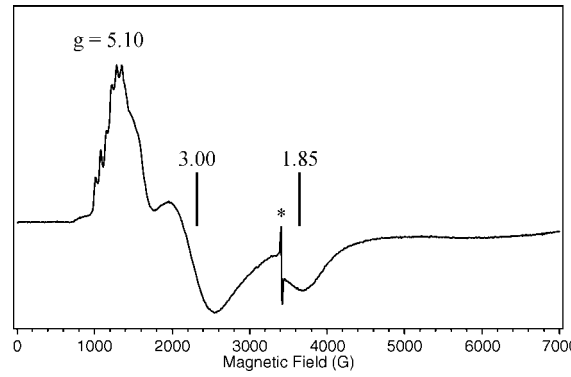

Figure 7. X-band EPR spectra of $Cl-Mn^{IV}(salen)$ generated from **2** + 1.0 equiv of **3** at 4 K in frozen CH_2Cl_2-toluene (7:3). Conditions: microwave frequency, 9.56 GHz; microwave power, 2.012 mW; modulation amplitude, 7 G; time constant, 163.84 ms; conversion time, 163.84 ms. The sharp signal designated with an asterisk comes from remaining **3**.

These spectroscopic features are consistent with formation of a Mn^{IV} complex, rather than a Mn^{III}-phenoxyl radical species. An ESI-MS spectrum of $[\mathbf{2}]^+$ gives a single signal at *m*/*z* 1064.34 as a singly charged ion, which corresponds to $[Mn(salen)(Cl)]^+$. The EPR spectrum of $[\mathbf{2}]^+$ shown in Figure 7 exhibits one set of signals at $g = 5.10$, 3.00, and 1.85, which is typical of an $S_t = {}^3/_2$ spin system ($E/D \approx 0.20$).[8c,d] The signal at $g = 5.10$ displays a six-line hyperfine splitting with $A = 68.5$ G, as expected for the $I = {}^5/_2$ ^{55}Mn nucleus. The signals at $g = 5.10$, 3.00, and 1.85, which arise from the transition between the $m_s = \pm{}^1/_2$ levels of an $S = {}^3/_2$ spin system, show Curie-law behavior in the range of 2.3–50 K, thus indicative of the d^3 Mn^{IV} formation with a positive zero-field splitting value *D*. Variable-temperature EPR shows that the starting Mn^{III} precursor **2** is supposed to be an $S = 2$ spin system with a negative *D*,[8d] and thus, one-electron oxidation of **2** changes the sign of the *D* value from negative to positive. The combined spectroscopic data clearly indicate that $[\mathbf{2}]^+$ is Mn^{IV}-phenolate, $Cl-Mn^{IV}(salen)$.

Interestingly, the addition of 1.0 equiv of $AgSbF_6$ to the CH_2Cl_2 solution of $Cl-Mn^{IV}(salen)$ at 203 K generates another distinct species, which is identified as the Mn^{III}-phenoxyl radical by UV–vis, EPR, and ^{2}H NMR spectra.

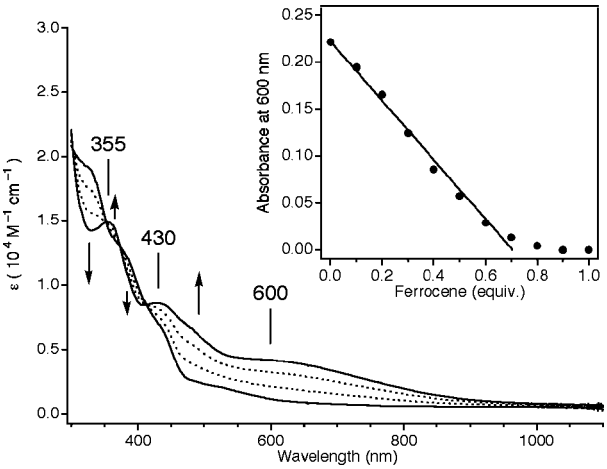

Figure 8. UV–vis spectral changes of **1** to O=Mn^{IV}(salen) upon reaction with O_3 in CH_2Cl_2 at 203 K. Inset: A plot of absorbance at 600 nm versus the equivalents of added ferrocene.

Removal of the Cl ligand on the fifth coordination site as AgCl and the coordination of an SbF_6^- counteranion or H_2O in solvent induce intramolecular electron transfer from phenolate to the Mn^{IV} center, resulting in conversion to the Mn^{III}-phenoxyl radical. This observation clearly indicates that the external ligand plays a primary role in determining the electronic structure of Mn(salen) in higher oxidation states.

O=Mn^{IV}(salen) and HO−Mn^{IV}(salen). O=Mn^{IV}(salen) was prepared by reaction of **1** with O_3, which is an oxidant frequently employed to generate high-valent metal-oxo species.[4c,19] Upon reaction with O_3 at 203 K, **1** shows absorption spectral changes with clear isosbestic points to generate a transient intermediate with absorptions at 355, 430, and 600 nm (Figure 8). The absorption spectrum of the transient intermediate is similar to that of Mn^{IV}-phenolate, Cl−Mn^{IV}(salen), rather than that of the Mn^{III}-phenoxyl radical, H_2O−Mn^{III}(salen$^{+\bullet}$). A redox titration of the transient intermediate with ferrocene indicates that this intermediate is in the one-electron oxidized state from **1**. A ^{2}H NMR measurement of this transient intermediate at 203 K shows broad NMR signals at 23.4 and −33.2 ppm (Figure S6, Supporting Information). The EPR spectrum shows signals at $g = 4.20$, 3.50, and 1.95, which arise from the transition between the $m_s = \pm 1/2$ levels of an $S_t = 3/2$ spin system ($E/D \approx 0.05$),[8c,d] and the signals show Curie-law behavior in the range of 2.3–50 K, indicative of a positive D. These ^{2}H NMR and EPR data for the transient intermediate are also consistent with formation of Mn^{IV} species, in comparison with those for Mn^{IV}-phenolate, Cl−Mn^{IV}(salen) versus the Mn^{III}-phenoxyl radical, H_2O−Mn^{III}(salen$^{+\bullet}$). ESI-MS spectrometry at low temperatures does not give any molecular ion peak, suggesting that this intermediate is a neutral complex. Attempts to detect Mn=O vibrations by resonance Raman spectroscopy with an excitation wavelength of 351.4, 413.1, or 600 nm or by Fourier transform infrared experiments were not successful.

The coordination structure of O=Mn^{IV}(salen) was investigated by XAS. As seen from the Mn K-edge X-ray absorption near-edge structure (XANES) regions (Figure 9a), the pre-edge height is not increased at all upon formation of O=Mn^{IV}(salen) from **1**, which is in contrast to significantly increased pre-edge heights for Mn^{V} complexes.[8e,20] Both the pre-edge and the absorption edge for O=Mn^{IV}(salen) is shifted to higher energy by 0.1 and 0.6 eV, respectively, compared with the Mn^{III} precursor **1** (Table 2). The extended X-ray absorption fine structure (EXAFS) spectrum of O=Mn^{IV}(salen) shows a clearly resolved peak at a phase-shifted distance $R' \approx 1$ Å, as shown in Figure 9b. Curve-fitting suggests that this peak corresponds to a bond distance

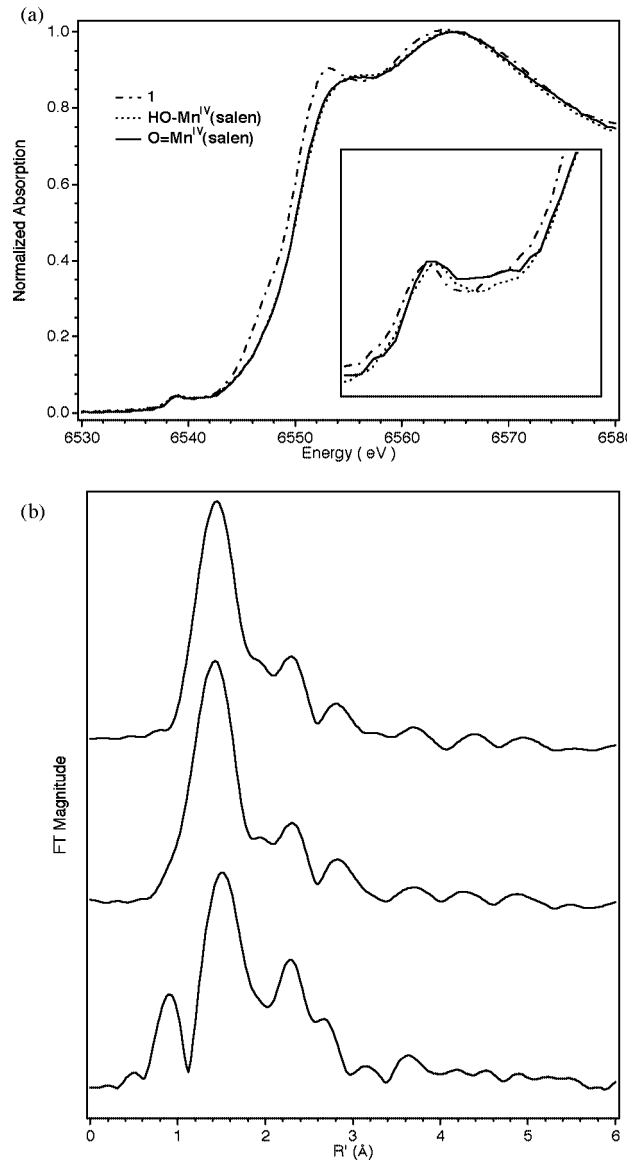

Figure 9. (a) XANES spectra of **1** (solid), HO−Mn^{IV}(salen), and O=Mn^{IV}(salen) (20 mM frozen propionitrile solution) at 10 K. Inset: The pre-edge region around 6540 eV. (b) The k^2-weighted Fourier transform magnitude of Mn K-edge EXAFS spectra of **1** (top), HO−Mn^{IV}(salen) (middle), and O=Mn^{IV}(salen) (bottom), calculated in the k range of 2–12 Å^{-1}.

(19) (a) Gross, Z.; Nimri, S. *Inorg. Chem.* **1994**, *33*, 1731–1732. (b) Fujii, H.; Yoshimura, T.; Kamada, H. *Inorg. Chem.* **1997**, *36*, 6142–6143.

(20) (a) Weng, T.-C.; Hsieh, W.-Y.; Uffelman, E. S.; Gordon-Wylie, S. W.; Collins, T. J.; Pecoraro, V. L.; Penner-Hahn, J. E. *J. Am. Chem. Soc.* **2004**, *126*, 8070–8071. (b) Lansky, D. E.; Mandimutsira, B.; Ramdhanie, B.; Clausén, M.; Penner-Hahn, J.; Zvyagin, S. A.; Telser, J.; Krzystek, J.; Zhan, R.; Ou, Z.; Kadish, K. M.; Zakharov, L.; Rheingold, A. L.; Goldberg, D. P. *Inorg. Chem.* **2005**, *44*, 4485–4498.

Table 2. XAS Edge Energies, Pre-Edge Energies, and Heights for **1**, HO−Mn^{IV}(salen), and O=Mn^{IV}(salen)

compd	edge energy (eV)[a]	pre-edge energy (eV)	pre-edge peak height
1	6549.3	6538.8	0.045
HO−Mn^{IV}(salen)	6549.9	6539.0	0.044
O=Mn^{IV}(salen)	6549.9	6538.9	0.046

[a] The edge positions were reported as those at a normalized absorption of 0.5.

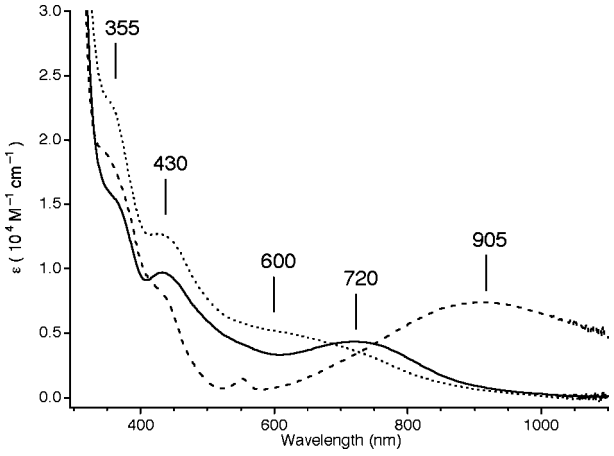

Figure 10. UV–vis spectral changes of H_2O−Mn^{III}(salen$^{+\bullet}$) (---) to HO−Mn^{IV}(salen) (—) and O=Mn^{IV}(salen) (···) upon addition of 1.0 equiv and 2.0 equiv of Bu_4NOH in CH_2Cl_2 at 203 K.

of 1.58 Å (Table 3), which is almost comparable to the value of 1.55 Å for the fully characterized Mn^V=O complexes.[9a–d] This peak, which is shorter than the other Mn−N/O_{salen} bonds, could be assigned as the Mn^{IV}=O bond. It is thus clearly indicated that the intermediate generated by reaction of **1** with O_3 is O=Mn^{IV}(salen). O≡Mn^V(salen), the most likely candidate for the reactive species for epoxidation, is not detected at all, probably because O≡Mn^V(salen) is so reactive as to be readily reduced even at 203 K.

HO−Mn^{IV}(salen) was prepared from H_2O−Mn^{III}(salen$^{+\bullet}$) by the addition of a base at low temperatures. Upon addition of 1.0 equiv of Bu_4NOH at 203 K, H_2O−Mn^{III}(salen$^{+\bullet}$) shows absorption spectral changes with isosbestic points at 420 and 715 nm, and the characteristic absorption at 905 nm completely diminishes along with a concomitant increase in absorption at 720 nm, as shown in Figure 10. Further addition of 1.0 equiv of Bu_4NOH induces slight spectral changes with an isosbestic point at 740 nm, resulting in a UV–vis spectrum with absorption maxima at 355, 430, and 600 nm, which is exactly the same as that for O=Mn^{IV}(salen). ^{2}H NMR and EPR spectroscopy also shows that the intermediate generated by the addition of 2.0 equiv of Bu_4NOH to H_2O−Mn^{III}(salen$^{+\bullet}$) is identical with O=Mn^{IV}(salen). On the other hand, the addition of 1.0 equiv of CF_3SO_3H to O=Mn^{IV}(salen) regenerates the intermediate with absorption at 720 nm, but further addition of CF_3SO_3H does not regenerate H_2O−Mn^{III}(salen$^{+\bullet}$).

The intermediate with absorption at 720 nm is Mn^{IV}-phenolate, not the Mn^{III}-phenoxyl radical, as clearly indicated from the absorption features and the well-resolved ^{2}H NMR signals (Figure S7, Supporting Information). This intermediate shows EPR signals at g = 5.10, 3.10, and 1.85, which arise from the transition between the $m_s = \pm 1/2$ levels of an $S_t = 3/2$ spin system ($E/D \approx 0.20$),[8c,d] and the signals obey the Curie law in the range of 2.3–50 K, indicative of a positive D. ESI-MS of this intermediate[21] gives a singly charged ion at m/z 1046.51, which corresponds to [Mn(salen)(OH)]$^+$, indicating formation of a Mn^{IV} complex bearing OH as an external ligand, HO−Mn^{IV}(salen). Comparison of the XANES regions (Figure 9a, Table 2) shows almost identical spectra for O=Mn^{IV}(salen) and HO−Mn^{IV}(salen), indicating closely similar electronic and coordination structures. However, the EXAFS spectrum of HO−Mn^{IV}(salen) is strikingly different from that of O=Mn^{IV}(salen) and shows no clear resolved peak at a phase-shifted distance $R' \approx 1$ Å (Figure 9b). In curve fitting of the EXAFS spectrum of HO−Mn^{IV}(salen), at most, two shells can be used due to a resolution. Upon formation of HO−Mn^{IV}(salen), the Mn−N/O_{salen} bond distances may not differ considerably, which is indeed the case for O=Mn^{IV}(salen). Then, the Mn^{IV}−OH bond may be grouped into the shorter shell (∼1.81 Å, N = 2) or the longer shell (∼1.99 Å, N = 2) from the Mn−N/O_{salen} bonds. We thus carried out two possible two-shell curve fittings as shown in Table 3, and the best fit gives a Mn^{IV}−OH bond of 1.83 Å, which is in agreement with the crystallographically determined Mn^{IV}−OH distance (1.81 Å) in a mononuclear Mn^{IV} complex with two OH ligands.[29b] Interconversions among all the intermediates described herein are summarized in Scheme 1.

Reactivity of O=Mn^{IV}(salen). Reactions of O=Mn^{IV}(salen) with various substrates were investigated at 223 K. At this temperature, O=Mn^{IV}(salen) in CH_2Cl_2 gradually decomposes ($t_{1/2} \approx 9$ h). O=Mn^{IV}(salen) is more stable in CD_2Cl_2 than in CH_2Cl_2 (k_H/k_D = 3.5), suggesting that hydrogen atom abstraction from CH_2Cl_2 molecules is one of the decomposition pathways. Reactions of O=Mn^{IV}(salen) with triphenylphosphine and methyl *p*-tolyl sulfide (100 equiv) in CH_2Cl_2 under an Ar atmosphere give triphenylphosphine oxide and methyl *p*-tolyl sulfoxide in 70 ± 15 and 8.8 ± 1% yields, respectively. The ^{18}O incorporation from the ^{18}O-labeled O=Mn^{IV}(salen) was found to be 24 and 39% for triphenylphosphine oxide and methyl *p*-tolyl sulfoxide, respectively. When the reaction is carried out under O_2 atmosphere, the yields of triphenylphosphine oxide and methyl *p*-tolyl sulfoxide are increased to 180 ± 15 and 39 ± 2%, suggesting that reactions of O=Mn^{IV}(salen) with phosphine and sulfide partially proceed by a radical chain mechanism. Reaction of O=Mn^{IV}(salen) with norbornylene was also examined. But the addition of norbornylene (100 equiv) to the CH_2Cl_2 solution of O=Mn^{IV}(salen) does not change the rate of disappearance of O=Mn^{IV}(salen). Indeed, the yield of exo-2,3-epoxynorbornane after 10 h is found to be less than 1%. Although O=Mn^{IV}(salen) does possess the ability of oxygen atom transfer toward phosphine and sulfide, the oxidizing power is not enough for epoxidation of olefins. This suggests that O=Mn^{IV}(salen) might not be a reactive intermediate for Jacobsen−Katsuki enantioselective epoxi-

(21) 2,6-Di-*tert*-butylpyridine is utilized instead of Bu_4NOH, because Bu_4NOH disturbs the ionization of analytes.

Table 3. EXAFS Curve Fitting Results for **1**, HO−Mn^{IV}(salen), and O=Mn^{IV}(salen)

compd		N^a	R (Å)^b	σ^2 (Å^2)^c	ΔE_0 (eV)^d	R (%)^e
1	$Mn-O_{external\_ligand}$	1	2.166	0.0024	3.96	11.8
	$Mn-N/O_{salen}$	1	1.847	0.0022	3.96	
		1	1.861	0.0021	3.96	
		1	1.983	0.00002	15.1	
		1	1.970	0.00002	15.1	
HO−Mn^{IV}(salen)	$Mn-O_{external\_ligand}$	1	1.83	−0.0025	6.71	3.84
	$Mn-N/O_{salen}$	2	1.83	−0.0025	6.71	
		2	1.98	−0.0063	8.11	
	$Mn-O_{external\_ligand}$	1	1.96	−0.0058	7.81	4.41
	$Mn-N/O_{salen}$	2	1.81	−0.0049	6.61	
		2	1.96	−0.0058	7.81	
O=Mn^{IV}(salen)	$Mn-O_{external\_ligand}$	1	1.58	−0.0020	−0.56	14.8
	$Mn-N/O_{salen}$	2	1.81	−0.0033	6.65	
		2	1.99	−0.0059	5.78	

[a] Coordination number, fixed at the value shown. [b] Interatomic distances estimated from EXAFS curve fitting for HO−Mn^{IV}(salen) and O=Mn^{IV}(salen), and those determined by X-ray crystal structural analysis for **1** (fixed parameter in the fitting). [c] Debye–Waller factor. [d] Shift in photoelectron energy zero. [e] R factors, defined as $\sum|y_{exp}(i) - y_{theo}(i)|/\sum|y_{exp}(i)|$, where y_{exp} and y_{theo} are experimental and theoretical data points, respectively.

Scheme 1

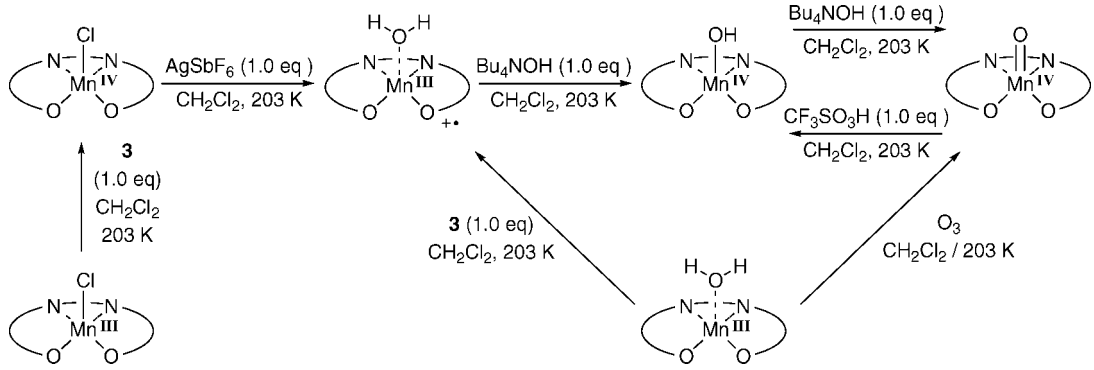

Table 4. Hydrogen Atom Abstraction from Selected Substrates by O=Mn^{IV}(salen)

substrate	BDE (kcal/mol)	product	yield (%)	k (s^{-1})
1,4-cyclohexadiene[a]	76[c]	benzene	28 ± 3	2.09×10^{-3}
9,10-dihydroanthracene[a]	78[c]	anthracene	3.0 ± 1.0	1.11×10^{-4}
cyclohexene[b]	81.6[d]	2-cyclohexen-1-ol	5.0 ± 1.1	6.46×10^{-5}
		2-cyclohexen-1-one	7.7 ± 0.7	

[a] 100 equiv of substrate was added to the CH_2Cl_2 solution of O=Mn^{IV}(salen). [b] 500 equiv of cyclohexene was added to the CH_2Cl_2 solution of O=Mn^{IV}(salen). [c] Ref 32. [d] Ref 43.

dation, although reactivity of the Mn^{IV}=O unit in less bulky Mn(salen) catalysts utilized for enantioselective epoxidation still remains to be investigated.

On the other hand, the addition of cyclohexene (500 equiv) to the CH_2Cl_2 solution of O=Mn^{IV}(salen) slightly increases the rate of disappearance of O=Mn^{IV}(salen), indicating that O=Mn^{IV}(salen) does react with cyclohexene. Analysis of the reaction mixture after 10 h revealed that major products are 2-cyclohexen-1-ol (5.0 ± 1.1%) and 2-cyclohexen-1-one (7.7 ± 0.7%). Cyclohexene oxide is generated as a minor product (1.2 ± 0.1%).[22] Other possible oxidation products such as 2-cyclohexen-1-one oxide and bicyclohexene are not detected. When the reaction is carried out under an O_2 atmosphere, the yields of 2-cyclohexen-1-ol and 2-cyclohexen-1-one are increased to 10 ± 1.5 and 15 ± 2.1%, respectively, but the yield of cyclohexene oxide remains at 1.2 ± 0.1%. When the ^{18}O-labeled O=Mn^{IV}(salen) is reacted with cyclohexene, no ^{18}O incorporation into 2-cyclohexen-1-ol and 2-cyclohexen-1-one is observed. Thus, the oxygen atom in 2-cyclohexen-1-ol and 2-cyclohexen-1-one is not derived from O=Mn^{IV}(salen) but most probably comes from oxygen gas, which might be contaminated during a long reaction. It is interesting to note that neither HO−Mn^{IV}(salen) nor H_2O-Mn^{III}(salen$^{+\bullet}$) gives those oxidation products at all.

O=Mn^{IV}(salen) was reacted with 9,10-dihydroanthracene and 1,4-cyclohexadiene. Anthracene and benzene are generated as major products, respectively. Table 4 summarizes yields of oxidation products and pseudo-first-order rate constants k for the decay of O=Mn^{IV}(salen) in the presence of the substrate. As the bond dissociation energy (BDE) of the C−H bond is increased, the reaction rate decreases. This is consistent with the hydrogen atom abstraction mechanism.

(22) Formation of 2-cyclohexen-1-ol and 2-cyclohexen-1-one exactly coincides with the decay of O=Mn^{IV} (salen), suggesting that both are indeed derived from O=Mn^{IV}(salen) (Figure S9). In contrast, the formation of cyclohexene oxide is saturated in the very beginning of the reaction, albeit in the presence of O=Mn^{IV}(salen). When O=Mn^{IV}(salen) is prepared via a ligand exchange from H_2O-Mn^{III}(salen) and 2 equiv of Bu_4NOH, reaction with cyclohexene produced 2-cyclohexen-1-ol and 2-cyclohexen-1-one exclusively. These observations suggest that cyclohexene oxide is not derived from O=Mn^{IV}(salen).

Discussion

Spectroscopic Features of Mn^{IV}-Phenolate versus Mn^{III}-Phenoxyl Radical. Absorption features in the visible region could be a fingerprint to distinguish between Mn^{IV}-phenolate and Mn^{III}-phenoxyl radical formulations. Mn^{IV}-phenolate, $Cl-Mn^{IV}$(salen), shows an intense absorption at 730 nm ($\varepsilon = 6022\ M^{-1}\ cm^{-1}$), which could be assigned to the phenolate-to-Mn^{IV} charge-transfer band. The phenolate-to-Mn^{IV} charge-transfer band is shifted to higher energy upon replacement of the fifth ligand from Cl (730 nm) to OH (720 nm), OMe (600 nm),[23] and =O (<600 nm). Consistent with our observation, Mn^{IV} complexes containing phenolate groups are reported to show intense absorption (ε = 2000–6000 $M^{-1}\ cm^{-1}$) in the range of 500–650 nm.[24] On the other hand, the Mn^{III}-phenoxyl radical, $H_2O-Mn^{III}(salen^{+\bullet})$, exhibits a broad absorption at 905 nm (ε = 7000 $M^{-1}\ cm^{-1}$). By analogy to our previous result on Fe(salen),[7] further one-electron oxidation of $H_2O-Mn^{III}(salen^{+\bullet})$ may most probably generate a Mn^{III}-diphenoxyl radical, $H_2O-Mn^{III}(salen^{2+\bullet\bullet})$, which shows an absorption of doubled intensity at 980 nm. According to the recent experimental and theoretical studies on metal-organic radical complexes by Wieghardt and Neese,[25] these absorptions at 905 and 980 nm are most likely assigned to intervalence charge transfer between the phenolate and the phenoxyl radical and ligand-to-ligand charge transfer between the phenoxyl radicals for $H_2O-Mn^{III}(salen^{+\bullet})$ and $H_2O-Mn^{III}(salen^{2+\bullet\bullet})$, respectively. But the only example of the Mn^{III}-phenoxyl radical complex from the *monophenolate* complex also shows an absorption maximum at 1015 nm (ε = 1800 $M^{-1}\ cm^{-1}$),[11a] and thus a metal-to-ligand charge transfer assignment may not be completely ruled out for the 905 nm band in the present case. Variable-temperature EPR could differentiate between Mn^{IV}-phenolate and the Mn^{III}-phenoxyl radical from the present Mn^{III}(salen). Temperature dependence of EPR signals from all of the Mn^{IV}(salen)'s investigated herein shows that transitions between the $m_s = \pm^1/_2$ levels are the lowest energy levels, thus indicative of positive D values. In contrast, $H_2O-Mn^{III}(salen^{+\bullet})$ exhibits EPR signals, which arise from transitions from both the $m_s = \pm^1/_2$ and $M_s = \pm^3/_2$ levels, and their temperature dependence reveals a negative D value because of the $M_s = \pm^3/_2$ level as the ground Kramers doublet and the $m_s = \pm^1/_2$ level as the excited-state doublet. Thus, one-electron oxidation of the Mn center in Mn^{III}(salen) changes the sign of the D value from negative to positive, while the D value remains negative upon one-electron oxidation of the phenolate in Mn^{III}(salen). But such correlations might be limited to the present system, because signs and magnitudes of D are dependent on coordination environments.[8d,11a,24d,e] EPR is also a sensitive probe for the fifth external ligand, and E/D values vary depending on Cl (~0.20), OH (~0.20), OMe (~0.07), and =O (~0.05) as an external fifth ligand. Interestingly, this trend is completely parallel to the UV–vis absorption shifts in the phenolate-to-Mn^{IV} charge-transfer band. The previous resonance Raman study showed that the C−O stretching of the phenoxyl radical (Y7a′) appeared at different positions depending on metal ions even in the same ligand system, and this was attributed to different extents of double-bond character of the phenoxyl radical C−O bond, which are influenced by metal ions.[26] Interestingly, in the case of phenoxyl radicals from Mn(salen) and Fe(salen), Y7a′ bands are observed at exactly the same position (1485 cm^{-1}), which may indicate that the natures of phenoxyl radicals from Mn^{III}(salen) and Fe^{III}(salen) are exactly the same, irrespective of different redox potentials and Lewis acidities of Mn and Fe.

In light of the present spectroscopic data, some previous observations might be worth re-examining. One is a report that describes two crystallographically characterized mononuclear Mn complexes with tridentate ONO coordination, which were assigned as Mn^{IV}-phenolate.[27] Quite interestingly, the CH_2Cl_2 solutions of these show absorptions at 640 nm (ε = 1945 $M^{-1}\ cm^{-1}$)/890 nm (ε = 1090 $M^{-1}\ cm^{-1}$) and 640 nm (ε = 3850 $M^{-1}\ cm^{-1}$)/970 nm (ε = 900 $M^{-1}cm^{-1}$), respectively. The absorptions at 640 nm are consistent with Mn^{IV}-phenolate, but the absorptions at 890 and 970 nm rather suggest the Mn^{III}-phenoxyl radical. This might indicate that the reported system contains an equilibrium between Mn^{IV}-phenolate and the Mn^{III}-phenoxyl radical in solution. Another example is a paper that reports a high-valent Mn(salen) species from Jacobsen's catalyst.[8e] Reaction of Jacobsen's catalyst with *m*-CPBA generates a transient intermediate with absorption at 684 nm (ε = 4000 $M^{-1}\ cm^{-1}$). This transient intermediate was assumed to be $Mn^{IV}(salen^{+\bullet})$ with the 684 nm absorption assigned as a salen ligand radical. However, the present study casts doubt on their

(23) MeO−Mn^{IV}(salen) was prepared by addition of 1 equiv of NaOMe in MeOH to $H_2O-Mn^{III}(salen^{+\bullet})$ in CH_2Cl_2 at 203 K. The electronic structure was confirmed by UV−vis, EPR, ^2H NMR, and ESI-MS spectroscopy (Figure S10).

(24) (a) Matsushita, T.; Hirata, Y.; Shono, T. *Bull. Chem. Soc. Jpn.* **1982**, *55*, 108–112. (b) Okawa, H.; Nakamura, M.; Kida, S. *Bull. Chem. Soc. Jpn.* **1982**, *55*, 466–470. (c) Chin, D.-H.; Saywer, D. T.; Schaefer, W. P.; Simmons, C. J. *Inorg. Chem.* **1983**, *22*, 752–758. (d) Hartman, J. R.; Foxman, B. M.; Cooper, S. R. *Inorg. Chem.* **1984**, *23*, 1381–1387. (e) Lynch, M. W.; Hendrickson, D. N.; Fitzgerald, B. J.; Pierpont, C. G. *J. Am. Chem. Soc.* **1984**, *106*, 2041–2049. (f) Tirant, M.; Smith, T. D. *Inorg. Chim. Acta* **1986**, *121*, 5–11. (g) Kessissoglou, D. P.; Li, X.; Butler, W. M.; Pecoraro, V. L. *Inorg. Chem.* **1987**, *26*, 2487–2492. (h) Chandra, S. K.; Basu, P.; Ray, D.; Pal, S.; Chakravorty, A. *Inorg. Chem.* **1990**, *29*, 2423–2428. (i) Mikuriya, M.; Jie, D.; Kakuta, Y.; Tokii, T. *Bull. Chem. Soc. Jpn.* **1993**, *66*, 1132–1139. (j) Adam, B.; Bill, E.; Bothe, E.; Goerdt, B.; Haselhorst, G.; Hildenbrand, K.; Sokolowski, A.; Steenken, S.; Weyhermüller, T.; Wieghardt, K. *Chem.—Eur. J.* **1997**, *3*, 308–319.

(25) (a) Herebian, D.; Bothe, E.; Neese, F.; Weyhermüller, T.; Wieghardt, K. *J. Am. Chem. Soc.* **2003**, *125*, 9116–9128. (b) Herebian, D.; Wieghardt, K. E.; Neese, F. *J. Am. Chem. Soc.* **2003**, *125*, 10997–11005. (c) Blanchard, S.; Neese, F.; Bothe, E.; Bill, E.; Weyhermüller, T.; Wieghardt, K. *Inorg. Chem.* **2005**, *44*, 3636–3656. (d) Ray, K.; Begum, A.; Weyhermüller, T.; Piligkos, S.; van Slageren, J.; Neese, F.; Wieghardt, K. *J. Am. Chem. Soc.* **2005**, *127*, 4403–4415. (e) Ray, K.; Weyhermüller, T.; Neese, F.; Wieghardt, K. *Inorg. Chem.* **2005**, *44*, 5345–5360. (f) Chlopek, K.; Bothe, E.; Neese, F.; Weyhermüller, T.; Wieghardt, K. *Inorg. Chem.* **2006**, *45*, 6298–6307. (g) Kokatam, S.; Ray, K.; Pap, J.; Bill, E.; Geiger, W. E.; LeSuer, R. J.; Rieger, P. H.; Weyhermüller, T.; Neese, F.; Wieghardt, K. *Inorg. Chem.* **2007**, *46*, 1100–1111.

(26) Itoh, S.; Kumei, H.; Nagatomo, S.; Kitagawa, T.; Fukuzumi, S. *J. Am. Chem. Soc.* **2001**, *123*, 2165–2175.

(27) Dutta, S.; Basu, P.; Chakravorty, A. *Inorg. Chem.* **1991**, *30*, 4031–4037.

(28) Green, M. T.; Dawson, J. H.; Gray, H. B. *Science* **2004**, *304*, 1653–1656.

assignment, because the 684 nm absorption most likely originates from a phenolate-to-Mn^{IV} charge transfer, not a phenoxyl radical (a salen ligand radical). The present spectroscopic consideration could also provide a foundation for future investigations on the long-sought but still unknown intermediate in Jacobsen−Katsuki enantioselective epoxidation.

Mononuclear Mn^{IV}=O and Mn^{IV}−OH from Mn(salen). In spite of their importance as key intermediates postulated in both artificial and enzymatic reactions, very few Mn^{IV} species with terminal oxo ligands are thoroughly characterized,[6a–c,9f] thus limiting our knowledge of their structures and reactivity. The most important finding in this context is that O=Mn^{IV}(salen) is readily interconverted to HO−Mn^{IV}(salen) via an acid–base equilibrium. Although their spectroscopic properties including UV–vis and EPR are similar, EXAFS analysis clearly shows a shorter Mn−O bond for O=Mn^{IV}(salen) by 0.25 Å compared with HO−Mn^{IV}(salen) (1.58 versus 1.83 Å). The previous XAS study reveals that chloroperoxidase compound II (CPO-II) bears an Fe^{IV}−OH bond (1.82 Å), instead of an Fe^{IV}=O one (ca. 1.65 Å).[28] Then, the increase in the M^{IV}=O bond length upon protonation is similar between Mn and Fe complexes. In Fe^{IV}=O chemistry,[5] isolation and characterization of the Fe^{IV}−OH unit instead of Fe^{IV}=O in CPO-II is a rather special case, and this was attributed to strong axial electron donation by thiolate ligation.[28] On the other hand, protonation of the present O=Mn^{IV}(salen) is a consequence of basicity of the oxo ligand in the Mn^{IV}=O unit, which was already discussed in detail by Groves and Spiro.[6a] Indeed, there have been other examples, in which Mn^{IV}−OH species were isolated and characterized instead of Mn^{IV}=O.[29] The Mn−O bond length in the present five-coordinate O=Mn^{IV}(salen) (1.58 Å) is shorter than that in the five-coordinate O=Mn^{IV}(porphyrin) (1.69 Å), which was previously estimated by the EXAFS analysis.[6c] This might be possibly ascribed to a difference in coordination environments between salens and porphyrins, or to the slightly distorted square-pyramidal geometry in the present sterically hindered Mn(salen).

Another point to be noted is the pre-edge features for the present O=Mn^{IV}(salen). The present O=Mn^{IV}(salen) shows a pre-edge and an absorption edge shifted to higher energy by 0.1 and 0.6 eV, respectively, and the intensity of the pre-edge of O=Mn^{IV}(salen) is not increased significantly, compared with the Mn^{III} precursor **1**. The shift of the absorption edge to higher energy by 0.6 eV is consistent with the change in the oxidation state from Mn^{III} to Mn^{IV}, but a small change in the pre-edge feature may require particular attention in comparison with previous results. However, we can rule out X-ray damage such as photoreduction of O=Mn^{IV}(salen) during synchrotron radiation, which might cause a rather small change in the pre-edge feature, because no appreciable difference was observed for the first and the final data in the present XAS data, which are composed of 10 different sequential measurements for the same sample. In the absence of an authentic Mn^{IV}=O complex, which is crystallographically characterized and is subjected to a thorough XAS study, the XAS data for the crystallographically characterized O≡Mn^{V}(HMPA-B) complex is best for comparison (H_4(HMPA-B) = 1,2-bis(2-hydroxy-2-methylpropanamido)benzene).[20a] Upon formation of Mn^{V}≡O from Mn^{III}, the pre-edge transition is shifted to higher energy by 1.21 eV. Because the pre-edge energy shift on forming Mn^{IV}=O from Mn^{III} is then expected to be less than 1.21 eV, the pre-edge energy shift of 0.1 eV for the present case is somewhat small but does not fall far away from the expected range. It is also noted that different measurement conditions for **1** as a solid and O=Mn^{IV}(salen) in solution might be a possible cause for a small pre-edge energy change.

According to the quantitative consideration of the pre-edge intensity of metal-oxo complexes by Pecoraro and Penner-Hahn,[20a] formation of d^2 O≡Mn^{V}(HMPA-B) from Mn^{III} accompanies a ca. 9-fold increase in pre-edge intensity, which is also observed for the crystallographically characterized d^2 O≡Cr^{IV}(porphyrin).[30a] The crystallographically characterized d^4 O=Fe^{IV}(TMC) complex also shows an increase in pre-edge intensity,[30c] which is 6 times smaller than the increase in the case of the d^2 O≡Mn^{V}(HMPA-B) and O≡Cr^{IV}(porphyrin) complex (TMC = tetra(*N*-methyl)cyclam). The recent study on the O≡Fe^{V}(B) complex shows a 3-fold increase in the pre-edge intensity upon forming d^3 Fe^{V}≡O from Fe^{III} (H_4B = 3,3,6,6,9,9-hexamethyl-3,4,8,9-tetrahydro-1H-1,4,8,11-benzotetraazacyclotridecine-2,5,7,10(6H,11H)-tetraone).[31] In contrast, it was reported very recently by Nam et al. that the pre-edge intensity is not increased at all upon formation of the six-coordinate O≡Mn^{V}(porphyrin) from its Mn^{III} precursor.[6e] Thus, the extent of increase in pre-edge intensity varies depending on an electronic configuration and symmetry around the metal center in metal-oxo complexes. A precise explanation for the low pre-edge intensity in the present d^3 O=Mn^{IV}(salen) may be difficult at present, but several possibilities could be pointed out. One is symmetry around the metal center, which does affect pre-edge intensity.[6e,30b] Although the present O=Mn^{IV}(salen) does not possess a trans axial ligand, the coordination geometry might be distorted from square-pyramidal upon forming Mn^{IV}=O due to steric hindrance, resulting in a more centrosymmetric metal center than other metal-oxo species. Another is a spin state of a metal center, d^3 Mn^{IV}=O of $S = {}^3/_2$ versus d^3 Fe^{V}≡O of $S = {}^1/_2$. The high-spin configuration in the present O=Mn^{IV}(salen) might disturb Mn(3d) + O(2p) orbital mixing, a major factor in facilitating a normally forbidden 1s → 3d pre-edge transition in metal-oxo complexes, thus resulting in a lower pre-edge intensity.

(29) (a) Makino, R.; Uno, T.; Nishimura, Y.; Iizuka, T.; Tsuboi, M.; Ishimura, Y. *J. Biol. Chem.* **1986**, *261*, 8376–8382. (b) Yin, G.; McCormick, J. M.; Buchalova, M.; Danby, A. M.; Rodgers, K.; Day, V. W.; Smith, K.; Perkins, C. M.; Kitko, D.; Carter, J. D.; Scheper, W. M.; Busch, D. H. *Inorg. Chem.* **2006**, *45*, 8052–8061.

(30) (a) Penner-Hahn, J. E.; Benfatto, M.; Hedman, B.; Takahashi, T.; Doniach, S.; Groves, J. T.; Hodgson, K. O. *Inorg. Chem.* **1986**, *25*, 2255–2259. (b) Westre, T. E.; Kennepohl, P.; DeWitt, J. G.; Hedman, B.; Hodgson, K. O.; Solomon, E. I. *J. Am. Chem. Soc.* **1997**, *119*, 6297–6314. (c) Lim, M. H.; Rohde, J.-U.; Stubna, A.; Bukowski, M. R.; Costas, M.; Ho, R. Y. N.; Münck, E.; Nam, W.; Que, L., Jr *Proc. Natl. Acad. Sci. U.S.A.* **2003**, *100*, 3665–3670.

(31) Tiago de Oliveira, F.; Chanda, A.; Banerjee, D.; Shan, X.; Mondal, S.; Que, L. Jr.; Bominaar, E. L.; Münck, E.; Collins, T. J *Science* **2007**, *315*, 835–838.

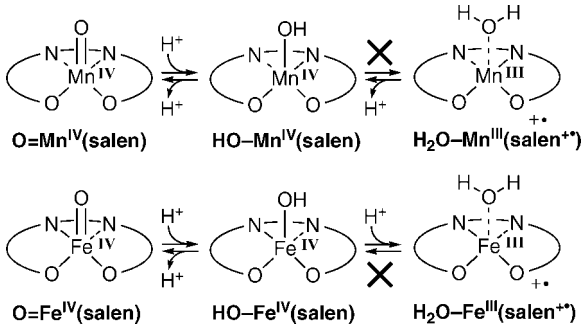

Figure 11. Acid–base equilibrium between Mn^{IV}−phenolate and Mn^{III}−phenoxyl radical for Mn(salen), in comparison with the case of Fe(salen).

Interconversion and Energetics between Mn^{IV}-Phenolate and Mn^{III}-Phenoxyl Radical as a Determinant Factor for Reactivity. Among O═Mn^{IV}(salen), HO−Mn^{IV}(salen), and H_2O−Mn^{III}($salen^{+\bullet}$), only O═Mn^{IV}(salen) shows hydrogen-abstracting ability. Protonation of O═Mn^{IV}(salen) reversibly generates HO−Mn^{IV}(salen), which shows considerably reduced hydrogen-abstracting ability. The reactivity difference between Mn^{IV}═O and Mn^{IV}−OH was also noted by Busch et al. very recently.[32] They compared rate constants for hydrogen-abstraction reactions with the fully characterized dihydroxo Mn^{IV} complex at pH 4.0 and 8.4 and found that reactions at pH 8.4 are ∼14 times faster than those at pH 4.0. The thermodynamic basis for the reactivity difference remains unknown, because estimated BDE values of OH bonds that form from Mn^{IV}═O and Mn^{IV}−OH are very similar. The present study reveals for the first time the structural difference between Mn^{IV}═O and Mn^{IV}−OH, which might be somewhat correlated with the peculiar reactivity difference. H_2O−Mn^{III}($salen^{+\bullet}$) is formally regarded as a diprotonated form of O═Mn^{IV}(salen), but the electronic structure is not Mn^{IV}-phenolate any more, but the Mn^{III}-phenoxyl radical instead, which has no hydrogen-abstracting ability for substrates such as cyclohexene. The most critical feature in relation to the catalytic activity of Mn(salen) is that the formation of inactive H_2O−Mn^{III}($salen^{+\bullet}$) is considerably unfavorable in energetics among O═Mn^{IV}(salen), HO−Mn^{IV}(salen), and H_2O−Mn^{III}($salen^{+\bullet}$) (Figure 11). Indeed, H_2O−Mn^{III}($salen^{+\bullet}$) is readily converted to HO−Mn^{IV}(salen) by addition of Bu_4NOH, while HO−Mn^{IV}(salen) cannot be converted back to H_2O−Mn^{III}($salen^{+\bullet}$) even in the presence of strong protic acid CF_3SO_3H.[33] Energetics that favor the generation of high-valent metal-oxo species is exactly the evidence for the high catalytic activity of Mn(salen).

In our previous study on Fe(salen), one-electron oxidation of both Fe^{III}(salen)(Cl) and Fe^{III}(salen)(H_2O) generates the Fe^{III}-phenoxyl radical.[7] Upon one-electron oxidation, Fe^{III}(salen)(OH) is readily protonated by a small amount of acid that might be formed by electrochemical water oxidation to give Fe^{III}(salen)(H_2O), which is then oxidized to the Fe^{III}-phenoxyl radical. Attempts to generate O═Fe^{IV}(salen) by reaction with *m*-CPBA also resulted in formation of the Fe^{III}-phenoxyl radical, and we did not observe any evidence for an Fe^{IV} species with Mössbauer spectroscopy. In the case of Fe(salen), the Fe^{III}-phenoxyl radical, H_2O-Fe^{III}($salen^{+\bullet}$), would be a thermodynamic sink (Figure 11). High-valent species O═Fe^{IV}(salen) and HO−Fe^{IV}(salen), which are candidates for potent oxidants, are readily converted to inactive H_2O−Fe^{III}($salen^{+\bullet}$) via protonation and intramolecular electron transfer. The absence of even trace Fe^{IV} species might indicate that generation of inactive H_2O−Fe^{III}($salen^{+\bullet}$) is considerably favored in energetics among O═Fe^{IV}(salen), HO−Fe^{IV}(salen), and H_2O−Fe^{III}($salen^{+\bullet}$), which results in no catalytic activity of Fe(salen). Such energetics between high-valent and ligand-radical species could also determine the oxidizing activity of metal ions in porphyrin and other ligand systems.

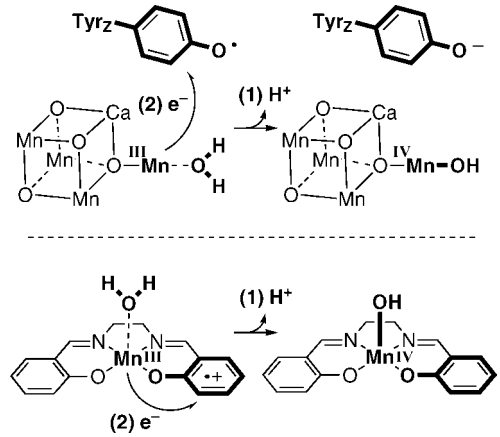

Figure 12. Relevance of the present model system to the photosynthetic water oxidation by the OEC complex.

Relevance to Photosynthetic Water Oxidation by the OEC Complex. One of the key steps in photosynthetic water oxidation is sequential one-electron oxidations and proton transfers mediated by the uncoordinated tyrosyl radical (Tyr_Z), which is positioned at ∼5.0 Å away from the Mn center and is proposed to function as a hydrogen atom abstractor.[34] The present model system, which has a phenoxyl radical coordinated to the Mn^{III} center and which exhibits conversion from H_2O−Mn^{III}($salen^{+\bullet}$) to HO−Mn^{IV}(salen) via proton and electron transfer, is thus quite relevant (Figure 12). Among other related model systems,[35] the present model is the first to evaluate the energetics between Mn^{IV}-phenolate and the Mn^{III}-phenoxyl radical. When water is bound on Mn as H_2O, one-electron oxidation of Mn(salen) generates the Mn^{III}-phenoxyl radical. But once H_2O on Mn is deprotonated to OH, the Mn^{III}-phenoxyl radical is readily converted to more stable Mn^{IV}-phenolate via intramolecular electron transfer from the Mn^{III} center to the phenoxyl radical.

(32) Yin, G.; Danby, A. M.; Kitko, D.; Carter, J. D.; Scheper, W. M.; Busch, D. H. *J. Am. Chem. Soc.* **2007**, *129*, 1512–1513.

(33) As demonstrated in the conversion of Cl−Mn^{IV}(salen) to H_2O−Mn^{III}($salen^{+\bullet}$), reversed electron transfer indeed occurs from the phenolate to the Mn^{IV} center. In this case, the thermodynamically unfavorable process is enforced by removal of Cl as an AgCl precipitate from the equilibrium system.

(34) Hoganson, C. W.; Babcock, G. T. *Science* **1997**, *277*, 1953–1956.

(35) (a) Pecoraro, V. L.; Baldwin, M. J.; Caudle, M. T.; Hsieh, W.-Y.; Law, N. A. *Pure Appl. Chem.* **1998**, *70*, 925–929. (b) Gupta, R.; Borovik, A. S. *J. Am. Chem. Soc.* **2003**, *125*, 13234–13242. (c) Maneiro, M.; Ruettinger, W. F.; Bourles, E.; McLendon, G. L.; Dismukes, G. C. *Proc. Natl. Acad. Sci. U.S.A.* **2003**, *100*, 3707–3712. (e) Mayer, J. M.; Rhile, I. J.; Larsen, F. B.; Mader, E. A.; Markle, T. F.; DiPasquale, A. G. *Photosynth. Res.* **2006**, *87*, 3–20.

Therefore, the present model suggests a proton and electron transfer mechanism, in which deprotonation of the Mn-bound H_2O triggers the electron transfer from Mn to Tyr_Z. It is interesting to note that a recent time-resolved X-ray study on the OEC complex argues against the validity of the hydrogen atom abstraction model and leads to a proposal of an alternative mechanism, in which Tyr_Z brings an electrostatic effect on the Mn-bound H_2O to induce a deprotonation reaction that is a prerequisite to the subsequent electron transfer to Tyr_Z.[36] Notably, the Fe complex in the same salen framework generates the Fe^{III}-phenoxyl radical irrespective of an external ligand, and electron transfer from the Fe^{III} center to the phenoxyl radical does not occur in any case.[7] Photosynthetic water oxidation is carried out exclusively by the Mn center, not by Fe, possibly due to feasible electron transfer from the Mn center to the tyrosyl radical.

Conclusion

We described herein the selective preparation and thorough characterization of O═Mn^{IV}(salen), HO−Mn^{IV}(salen), and H_2O−Mn^{III}(salen$^{+\bullet}$). O═Mn^{IV}(salen) shows oxygen atom transfer and hydrogen atom abstraction abilities, while HO−Mn^{IV}(salen), which only differs in the degree of protonation, but bears a longer Mn−O bond compared to O═Mn^{IV}(salen), shows reduced oxidizing activity. Poor oxidizing species H_2O−Mn^{III}(salen$^{+\bullet}$), which is also in a one-electron oxidized state with H_2O as an external ligand, is not described as Mn^{IV}-phenolate but the Mn^{III}-phenoxyl radical, indicating that transition from active Mn^{IV}-phenolate to the inactive Mn^{III}-phenoxyl radical is controlled by the degree of protonation of the fifth oxygen ligand. Energetics among O═Mn^{IV}(salen), HO−Mn^{IV}(salen), and H_2O−Mn^{III}(salen$^{+\bullet}$) favor the generation of active O═Mn^{IV}(salen), which is exactly the key for high catalytic activity of Mn(salen). The present study not only reveals the electronic basis for the high catalytic activity of Mn(salen) far beyond Fe(salen) but also may provide valuable insight into the development of efficient oxidation catalysts in the future.

Experimental Section

Instrumentation. Cyclic voltammograms were measured with an ALS612A electrochemical analyzer. UV–vis spectra were recorded on an Agilent 8453 (Agilent Technologies) equipped with a USP-203 low-temperature chamber (UNISOKU). UV–vis measurements upon controlled-potential electrochemical oxidation were reported in the previous paper.[7] EPR spectra were recorded in a quartz cell (d = 5 mm) at 4 K on an E500 continuous-wave X-band spectrometer (Bruker) with an ESR910 helium-flow cryostat (Oxford Instruments). Resonance Raman spectra were measured with a quartz spinning cell kept at 193 K, using an MC-100DG 100 cm single polychromator (Ritsu Ohyo Kogaku) equipped with an LN/CCD-1100-PB liquid-nitrogen-cooled CCD detector (Roper Scientific). A BeamLok 2080 argon ion laser (Spectra Physics) was utilized as an excitation source. The laser power at the sample was about 10 mW. Raman shifts were calibrated with indene. ESI-MS spectra were obtained with an LCT time-of-flight mass spectrometer equipped with an electrospray ionization interface (Micromass). The low-temperature ESI-MS method was reported previously.[7] The 500 MHz NMR spectra were measured on an LA-500 spectrometer (JEOL). Elemental analyses were conducted on a CHN corder MT-6 (Yanaco). Gas chromatography–mass spectroscopy (GC-MS) analysis was performed on a QP-5000 GC-MS system (Shimadzu) equipped with a capillary gas chromatograph (GC-17A, CBP5-M25–025 capillary column). Quantitative analysis was performed with GC-MS using undecane or benzophenone as an internal standard. Experiments were repeated three times, and averaged yields relative to **1** were reported.

XAS Measurements. Mn K-edge XAS data were obtained at SPring-8, beam line BL01B1, under ring conditions of 8 GeV and ca. 100 mA (Proposal No. 2007A1090). The XAS datum of **1** in the solid state was collected at room temperature, and the XAS data of O═Mn^{IV}(salen) and HO−Mn^{IV}(salen) in frozen propionitrile solution were collected at 10 K. The data collections were carried out in fluorescence mode with a Lytle detector, using a Si(111) double-crystal monochromator. A Cu foil was utilized to calibrate the energy. In the present XAS data, which are composed of 10 different sequential measurements for the same sample, the first and the final data were carefully compared, but no appreciable difference was observed, suggesting no X-ray damage such as photoreduction during synchrotron radiation.

The XAS data were Fourier-transformed between k = 2 and 12 Å^{-1} and processed in a standard manner using WinXAS software (version 3.1).[37] Theoretical EXAFS signals were calculated using FEFF (version 8.4).[38] Structural parameters obtained by curve fittings are summarized in Table 3. The coordination number (N) was fixed as indicated in Table 3 in curve-fitting procedures. The other parameters, including the interatomic distance (R), the shift in photoelectron energy zero (ΔE_0), and the Debye–Waller factor (σ), were allowed to vary. Curve fitting for structurally characterized **1**, in which R was fixed, shows that parameters for O═Mn^{IV}(salen) and HO−Mn^{IV}(salen) were reasonably well-converged. Curve fittings were carried out only for atoms which are coordinated to Mn. Curve-fitting results are shown in Figure S8 (Supporting Information).

Materials. CH_2Cl_2 was purchased from Kanto as anhydrous solvent and was stored in the presence of 4A molecular sieves. To remove traces of HCl, CH_2Cl_2 was passed through activated alumina under an Ar atmosphere just before use. Bu_4NClO_4 was purchased from Kanto and was dried over P_2O_5 in vacuo. CD_2Cl_2 was purchased from Acros and was stored in the presence of 4A molecular sieves. CD_2Cl_2 was also passed through activated alumina under an Ar atmosphere just before use. Propionitrile (99%), $AgClO_4$·H_2O (99.999%), $AgSbF_6$ (98%), and phenol-d_6 were purchased from Aldrich and were used as received. *sec*-Butyllithium and silica gel (60N, spherical neutral, particle size 40–100 μm) were purchased from Kanto. Bu_4NBr_3 was purchased from TCI. $Mn(OAc)_2$·$4H_2O$ was purchased from Wako. $H_2{}^{18}O$ was purchased from Cambridge Isotope Laboratories. The oxidant, **3**, was prepared according to the reported method[39] and was assayed with titration by ferrocene. *m*-CPBA was purchased from Nacalai and was purified by washing with a phosphate buffer.[40] The purity of *m*-CPBA was checked with iodometry. The synthesis of bis(3,5-dimesitylsalicylidene)-1,2-dimesitylethylenediamine was already reported elsewhere.[15] The synthesis of bis(3,5-dimesitylsalicylidene)-

(36) Haumann, M.; Liebisch, P.; Müller, C.; Barra, M.; Grabolle, M.; Dau, H. *Science* **2005**, *310*, 1019–1021.
(37) Ressler, T. *J. Synchrotron Radiat.* **1998**, *5*, 118–122.
(38) Ankudinov, A. L.; Bouldin, C. E.; Rehr, J. J.; Sims, J.; Hung, H. *Phys. Rev. B: Condens. Matter Mater. Phys.* **2002**, *65*, 1041071–11.
(39) Schmidt, W.; Steckhan, E. *Chem. Ber.* **1980**, *113*, 577–585.
(40) Schwartz, N. N.; Blumbergs, J. H. *J. Org. Chem.* **1964**, *29*, 1976–1979.

1,2-dimesitylethylenediamine-d_4 was carried out in the same manner except for the formylation of 1,3-dimesityl-2-(methoxymethoxy)-benzene-d_3, in which *sec*-butyl-lithium was utilized instead of *n*-butyl-lithium. 2,4-Dibromophenol-d_3 was prepared by bromination of phenol-d_6 with Bu_4NBr_3.[41] **CAUTION!** *The perchlorate salts used in this study are potentially explosive and should be handled in a small amount with great care.*

Synthesis of 2. Following the method reported by Jacobsen and Zhang,[42] $Mn(OAc)_2 \cdot 4H_2O$ (251.2 mg, 1.02 mmol) was added to a solution of bis(3,5-dimesitylsalicylidene)-1,2-dimesitylethylenediamine (501 mg, 0.51 mmol) in dry ethanol (30 mL). The mixture was heated to reflux for 1 h. Then, ethanol was removed by rotary evaporation, and the residue was dissolved in CH_2Cl_2 (30 mL). The organic layer was washed with 0.1 M HCl aqueous solution (20 mL × 3) and saturated NaCl aqueous solution (20 mL × 1) and was dried over anhydrous Na_2SO_4. The solvent was removed by rotary evaporation, and the residue was purified by silica flash column chromatography (CH_2Cl_2/methanol 50:1). The residue obtained after evaporation was dissolved in a minimum amount of CH_2Cl_2 and was passed through a membrane filter (Cosmonice Filter S, Nacalai). The residue was further purified by precipitating from hot acetonitrile solution to give **2** (227.4 mg, 0.21 mmol). Anal. calcd for $C_{70}H_{74}N_2O_2ClMn \cdot H_2O$: C, 77.58; H, 7.07; N, 2.58. Found: C, 77.76; H, 6.90; N, 2.61.

Synthesis of 1. $AgClO_4 \cdot H_2O$ (29.2 mg, 0.13 mmol) in THF (1 mL) was added to a solution of **2** (136.4 mg, 0.13 mmol) in THF (5 mL). The mixture was stirred at room temperature for 30 min and was then filtered to remove AgCl precipitate. The solvent was removed by rotary evaporation, and the residue was dried in vacuo. The residue dissolved in a minimum amount of CH_2Cl_2 was passed through a membrane filter (Cosmonice Filter S, Nacalai). Crystallization from CH_2Cl_2-hexane gave **1** (79.8 mg, 0.070 mmol). Anal. calcd for $C_{70}H_{74}N_2O_6ClMn \cdot 2H_2O$: C, 72.12; H, 6.74; N, 2.40. Found: C, 72.17; H, 6.92; N, 2.56.

Preparations of $H_2O-Mn^{III}(salen^{+\bullet})$ and $Cl-Mn^{IV}(salen)$. The solution of 1.0 equiv of **3** dissolved in a minimum amount of CH_2Cl_2 was added to the CH_2Cl_2 solution of **1**, **2**, **1**-d_4, and **2**-d_4 at 193 K. The concentrations are 0.5 mM for UV–vis, 0.5 mM for ESI-MS, 1.0 mM for EPR, 2.0 mM for resonance Raman, and 10 mM for ^2H NMR. One-electron oxidations were accomplished immediately, and the samples were subjected to the physical measurements just after addition of **3**. For ESI-MS measurements, the solution was diluted with an excess of cold CH_2Cl_2. The solvent mixture of CH_2Cl_2/toluene (7:3) was utilized for EPR measurements.

Preparation of $O=Mn^{IV}(salen)$. The stream of O_3 and O_2 prepared by UV-irradiation to the O_2 gas was passed through the CH_2Cl_2 solution of **1** at 193 K. The concentrations are 0.5 mM for UV–vis, 0.5 mM for ESI-MS, 1.0 mM for EPR, 10 mM for ^2H NMR, and 20 mM for XAS. For ESI-MS measurements, the solution was diluted with an excess of cold CH_2Cl_2. The solvent mixture of CH_2Cl_2/toluene (7:3) was utilized for EPR measurements. The XAS sample was prepared in propionitrile.

Preparations of $O=Mn^{IV}(salen)$, $HO-Mn^{IV}(salen)$, $MeO-Mn^{IV}(salen)$, and $H_2O-Mn^{III}(salen^{+\bullet})$ via Ligand Exchange Reactions. For preparations of $O=Mn^{IV}(salen)$ and $HO-Mn^{IV}(salen)$, the solution of 1.0 and 2.0 equiv of Bu_4NOH dissolved in a minimum amount of CH_2Cl_2 was added to the CH_2Cl_2 solution of $H_2O-Mn^{III}(salen^{+\bullet})$ at 193 K. For preparation of $MeO-Mn^{IV}(salen)$, the solution of 1.0 equiv of NaOMe dissolved in a minimum amount of methanol was added to the CH_2Cl_2 solution of $H_2O-Mn^{III}(salen^{+\bullet})$ at 193 K. In order to convert $Cl-Mn^{IV}(salen)$ to $H_2O-Mn^{III}(salen^{+\bullet})$, the solution of 1.0 equiv of $AgSbF_6$ dissolved in a minimum amount of CH_2Cl_2 was added to the CH_2Cl_2 solution of $Cl-Mn^{IV}(salen)$ at 193 K. The concentrations are 0.5 mM for UV–vis, 0.5 mM for ESI-MS, 1.0 mM for EPR, 10 mM for ^2H NMR, and 20 mM for XAS. Ligand exchange reactions were accomplished immediately, and thereafter the samples were subjected to the physical measurements. For ESI-MS measurements, the solution was diluted with an excess of cold CH_2Cl_2. The solvent mixture of CH_2Cl_2/toluene (7:3) was utilized for EPR measurements. The XAS sample of $HO-Mn^{IV}(salen)$ was prepared in propionitrile. The CH_2Cl_2 solution of $^{18}O=Mn^{IV}(salen)$ was prepared from the ^{18}O-labeled **1**, **3**, and $Bu_4N^{18}OH$ in exactly the same manner as described above. The ^{18}O-labeled **1** was prepared by dissolving **1** (~50 mg) in $H_2{}^{18}O$ (0.1 mL) and anhydrous THF (0.9 mL) and then evaporating the solvent in vacuo. This procedure was repeated three times. $Bu_4N^{18}OH$ was prepared similarly.

Reactions of $O=Mn^{IV}(salen)$ with Various Substrates. The $O=Mn^{IV}(salen)$ solution was prepared by reaction of **1** (0.4 μmol) in CH_2Cl_2 (0.4 mL) with O_3. The resulting solution was frozen in liquid nitrogen and thawed at 193 K under a vacuum to remove excess O_3 gas. This freeze–thaw cycle was repeated five times, and finally Ar or O_2 gas was introduced to the reaction vessel. Then, the solution of substrate (40 μmol) in CH_2Cl_2 (40 μL), which was degassed via five freeze–thaw cycles just prior to use, was added to the $O=Mn^{IV}(salen)$ solution at 223 K. After being stirred for 5 min for triphenylphosphine, 30 min for 1,4-cyclohexadiene and 9,10-dihydroanthracene, 1 h for methyl *p*-tolyl sulfide, and 10 h for norbornylene and cyclohexene at 223 K under an Ar or O_2 atmosphere, the reaction was quenched by the addition of Bu_4NI (4 μmol) in degassed CH_2Cl_2 (20 μL). A quantitative analysis of products was carried out by GC-MS. The averaged yields of products were determined from three independent experiments and were reported relative to **1**. A blank experiment in the absence of **1** showed that no triphenylphosphine oxide was formed. The ^{18}O-labeled $O=Mn^{IV}(salen)$ intermediate, which was prepared as described above and was degassed via a freeze–thaw method, was subjected to reactions with substrates in exactly the same manner. The ^{18}O incorporation was determined by GC-MS.

Acknowledgment. We thank Mr. Seiji Makita (IMS) for elemental analysis and Dr. Hajime Tanida (JASRI/SPring-8) for assistance in the measurement of X-ray absorption spectra. This work was supported by grants from the Ministry of Education, Culture, Sports, Science and Technology, Japan, and from the Japan Science and Technology Agency, CREST.

Supporting Information Available: The ORTEP view (Figure S1) and crystallographic data (Table S1) of **1**, X-ray crystallographic files in CIF format for **1**, and Figures S2–S10. This material is available free of charge via the Internet at http://pubs.acs.org.

IC702061Y

(41) Kajigaeshi, S.; Kakinami, T.; Okamoto, T.; Nakamura, H.; Fujikawa, M. *Bull. Chem. Soc. Jpn.* **1987**, *60*, 4187–4189.
(42) Zhang, W.; Jacobsen, E. N. *J. Org. Chem.* **1991**, *56*, 2296–2298.
(43) Denisov, E. T.; Denisova, T. G. *Handbook of Antioxidants: Bond Dissociation Energies, Rate Constants, Activation Energies and Enthalpies of Reactions*, 2nd ed.; CRC Press: Boca Raton, FL, 2000.